

See discussions, stats, and author profiles for this publication at: <https://www.researchgate.net/publication/51979832>

Genomic Design of Strong Direct-Gap Optical Transition in Si/Ge Core/Multishell Nanowires

ARTICLE *in* NANO LETTERS · JANUARY 2012

Impact Factor: 13.59 · DOI: 10.1021/nl2040892 · Source: PubMed

CITATIONS

20

READS

19

4 AUTHORS:



Lijun Zhang

40 PUBLICATIONS 488 CITATIONS

[SEE PROFILE](#)



Mayeul d'Avezac

University College London

29 PUBLICATIONS 400 CITATIONS

[SEE PROFILE](#)



Jun-Wei Luo

Chinese Academy of Sciences

71 PUBLICATIONS 623 CITATIONS

[SEE PROFILE](#)



Alex Zunger

University of Colorado Boulder

768 PUBLICATIONS 50,908 CITATIONS

[SEE PROFILE](#)

Genomic Design of Strong Direct-Gap Optical Transition in Si/Ge Core/Multishell Nanowires

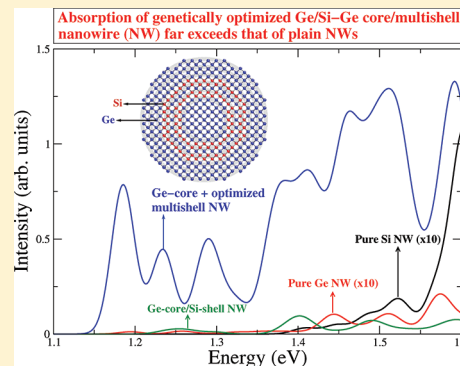
Lijun Zhang*,† Mayeul d'Avezac,† Jun-Wei Luo,† and Alex Zunger*,‡

†National Renewable Energy Laboratory, Golden, Colorado 80401, United States

‡University of Colorado, Boulder, Colorado 80302, United States

ABSTRACT: Finding a Si-based material with strong optical activity at the band-edge remains a challenge despite decades of research. The interest lies in combining optical and electronic functions on the same wafer, while retaining the extraordinary know-how developed for Si. However, Si is an indirect-gap material. The conservation of crystal momentum mandates that optical activity at the band-edge includes a phonon, on top of an electron–hole pair, and hence photon absorption and emission remain fairly unlikely events requiring optically rather thick samples. A promising avenue to convert Si-based materials to a strong light-absorber/emitter is to combine the effects on the band-structure of both nanostructuring and alloying. The number of possible configurations, however, shows a combinatorial explosion. Furthermore, whereas it is possible to readily identify the configurations that are formally direct in the momentum space (due to band-folding) yet do not have a dipole-allowed transition at threshold, the problem becomes not just calculation of band structure but also calculation of absorption strength. Using a combination of a genetic algorithm and a semiempirical pseudopotential Hamiltonian for describing the electronic structures, we have explored hundreds of thousands of possible coaxial core/multishell Si/Ge nanowires with the orientation of [001], [110], and [111], discovering some “magic sequences” of core followed by specific Si/Ge multishells, which can offer both a direct bandgap and a strong oscillator strength. The search has revealed a few simple design principles: (i) the Ge core is superior to the Si core in producing strong bandgap transition; (ii) [001] and [110] orientations have direct bandgap, whereas the [111] orientation does not; (iii) multishell nanowires can allow for greater optical activity by as much as an order of magnitude over plain nanowires; (iv) the main motif of the winning configurations giving direct allowed transitions involves rather thin Si shell embedded within wide Ge shells. We discuss the physical origin of the enhanced optical activity, as well as the effect of possible experimental structural imperfections on optical activity in our candidate core/multishell nanowires.

KEYWORDS: Silicon, light-emitting/absorbing, core/shell nanowire, genetic algorithm



Converting the electronically superior but optically impractical indirect-gap Si and Ge semiconductors into a strongly light-emitting/absorbing system has been a long-standing challenge accompanying the historical quest for optoelectronic devices based on column IV materials.^{1–12} The underlying problem is that whereas the valence band maximum (VBM), where holes (h) reside, is located in both Si and Ge at the center (Γ_h) of the fcc Brillouin zone, the conduction band minimum (CBM), where electrons (e) reside, is located off-gamma at K_e (in Si at the Δ_e point between Γ and X and in Ge at L_e), so electron–hole recombination violates momentum conservation unless a phonon of the appropriate momentum ($K_e - \Gamma_h$) is available. One of main approaches to create a visible optical transition without the need of a phonon has been the use of quantum confinement, zone folding and interband coupling afforded by two-dimensional (2D) layer-by-layer growth of Si/Ge superlattices.^{3–5,9,13–16} Here, one searches a sequence of 2D layers of $Si_p/Ge_q/Si_p/Ge_q\dots$ with atomic layer thicknesses ($p, q, p', q' \dots$) grown on a substrate with lattice constant a_s along some crystallographic direction (h, k, l), so that the electron state at K_e is relocated into $\bar{\Gamma}_e$ of the superlattice

Brillouin zone and, at the same time, the VBM-to-CBM transition has a direct-gap-like strong optical matrix element. The enormity of the parameter space [$(p, q, p', q' \dots) + a_s + (h, k, l)$] that needs to be searched, coupled with the practical limitations in coherently growing a 2D superlattice on a substrate with a generally mismatched a_s have severely limited the number of cases that could be explored over the years.^{3–5,14,15} The best 2D superlattice candidate found empirically from a very limited search was Si_6Ge_4 grown on partly relaxed, $Si_{1-x}Ge_x$ alloy, [001]-oriented buffer layer,⁴ which, despite having a direct VBM-to-CBM transition, had a disappointingly much weaker optical transition than that in direct-gap materials. Recently, a much more complete theoretical search, using genetic algorithm¹⁷ has resulted in a very different prediction of a direct-gap 2D superlattice: $Si_1Ge_2Si_2Ge_2Si_1Ge_n$ grown on [001] $Si_{1-x}Ge_x$ substrate with $x \geq 0.6$. It has been predicted to have a ~50 fold stronger optical

Received: November 21, 2011

Revised: December 19, 2011

Published: January 3, 2012

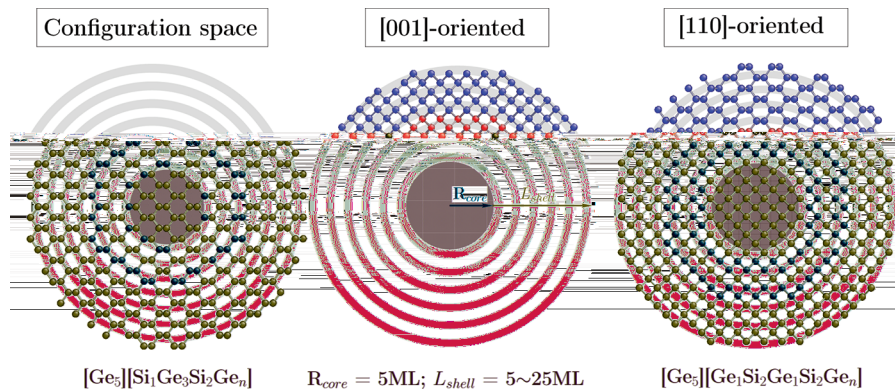


Figure 1. Scratch of configuration space (i.e., the cross-section of Si/Ge NW with a core and multishells) used in GA search (left) and best individuals with highest oscillator strength for [001]-oriented (middle) and [110]-oriented (right) NWs. Parameters of configuration space: core radius R_{core} = 5 ML; shell thickness L_{shell} = (5, 25) ML; core and each shell being either Si or Ge. The composition formula of best individuals shown represents the sequence of Si/Ge monolayers along the radial direction (starting from the NW axis). For [110]-oriented NWs, apart from the best individual shown, $[Ge_5][Si_1Ge_3Si_2Ge_n]$ (labeled as best GA NW I), another closely related individual with the inner single-layer Si replaced by a single-layer Ge (i.e., $[Ge_5][Ge_4Si_2Ge_n]$) (labeled as best GA NW II)), also show competitively strong oscillator strength (see Table 1).

transition than the best previous Si_6Ge_4 record calculated in the same way. Growth of such a structure is yet to be attempted.

If the target superlattice has an equilibrium (“free floating”) in-plane lattice constant of a_{SL} , the maximum thickness that can be grown coherently (dislocation-free) on a substrate with in-plane a_S is limited by the lattice-mismatch-induced strain, $\varepsilon = (a_{SL} - a_S)/a_S$.¹⁸ This strong limitation can be partially relaxed by changing from 2D superlattice to one-dimensional (1D) quantum nanowire (NW) with coaxial core and a sequence of shells. Due to the cylinder-like curved interface geometry and comparable volume of core and shell segments, effective atomic relaxation can take place and much higher strain can be accommodated,^{19,20} hence permitting more flexibility when growing such 1D coaxial heterostructures. Furthermore, compared with vapor phase depositing in high vacuum chamber needed in molecular beam epitaxy (MBE) used for growing 2D superlattices, NWs can be readily grown using the simpler vapor–liquid–solid (VLS) technique.^{21–23} This requires a catalytic liquid alloy to rapidly adsorb a vapor precursor and grows single crystalline at the liquid–solid interface. VLS-based growth of Si/Ge core–shell and core–multishell NWs have demonstrated a significant level of synthetic control^{24,25} and attracted considerable interest for application in field-effect transistors.^{26,27} Recently, high-quality single-crystalline Si/Ge core/multishell NWs were grown with the formation of uniform and smooth shells in a layer-by-layer mode.²⁸ This demonstrates the possibility of further atomic-level engineering toward nanoscale Si/Ge-based opto-electronics.

Sufficient reduction in the symmetry of bulk Si and Ge, along with finite-size truncation are expected to relax the band structure rules controlling the forbidden VBM-CBM transition. This is demonstrated by the strong visible photoluminescence in porous Si and nanocrystalline Si/Ge.^{1,2,29} Though the underlying physical mechanism of such intensive light emissions is still under debate, quantum confinement was believed to play an important role.^{30,31} Visible photoluminescence was also reported in Si^{32–37} and Ge³⁸ NWs, usually accompanied by broad peak profile and size-tunable wavelength. Si NWs have exhibited additional advantages for potential light-emitters, such as significant suppression of nonradiative Auger recombination,³⁹ and very high linear

polarization anisotropy resulting from the large dielectric contrast between NWs and surrounding environment.^{32,33,40}

We have explored here the use of quantum NW geometry to achieve both a direct gap and a strong dipole-allowed optical transition matrix element in the Si/Ge system. The configuration space considered (left panel of Figure 1) consists of up to 25 concentric shell monolayers (MLs) each being either Si or Ge, matching up a NW core with the axis oriented along the [001], [110], or [111] direction. We use a genomic approach whereby a large number of atomic configurations ($2^{26} \cong 10^8$) are explored via a biologically inspired genetic algorithm (GA) which guides quantum-mechanical calculations of the electronic and optical properties in search of the winning configuration. We find that (i) [001] and [110]-oriented NWs have direct optical transitions, whereas [111]-oriented NWs are indirect, (ii) a Ge core is better than a Si core in producing strong bandgap absorption, (iii) the core/multishell heterostructures with designed configurations have great advantage over pure Si, Ge, core/single-shell, and homogeneous alloy NWs, (iv) strong optical transitions are found for rather narrow Si shell embedded in wide Ge shells. The present work provided useful design rules that can guide fabrication of such a system as an efficient Si/Ge-based light-emitting device.

METHOD

Core/multishell NWs are constructed by cutting infinite circular cylinders from diamond structure and are passivated by a fictitious lattice-matched barrier material with large bandgap in order to remove surface states from the NW bandgap. The NW diameter and shell thickness are given in units of atomic ML along [001] direction (1 ML = $1/a_{bulk}$, where a_{bulk} is the lattice constant of bulk Si/Ge). Lattice-mismatch (4% for Si/Ge) induced strains are optimized coherently between core and shells as addressed experimentally,²⁴ with a generalized valence force field functional parametrized for diamond Si/Ge by fitting the results of density functional theory (DFT).⁴¹ The electronic structures (single-particle energies and wave functions) of NWs are calculated via the atomistic pseudopotential method developed for large-scale nanostructure calculations as described in ref 42. For each NW configuration, we numerically solve the Schrödinger equation

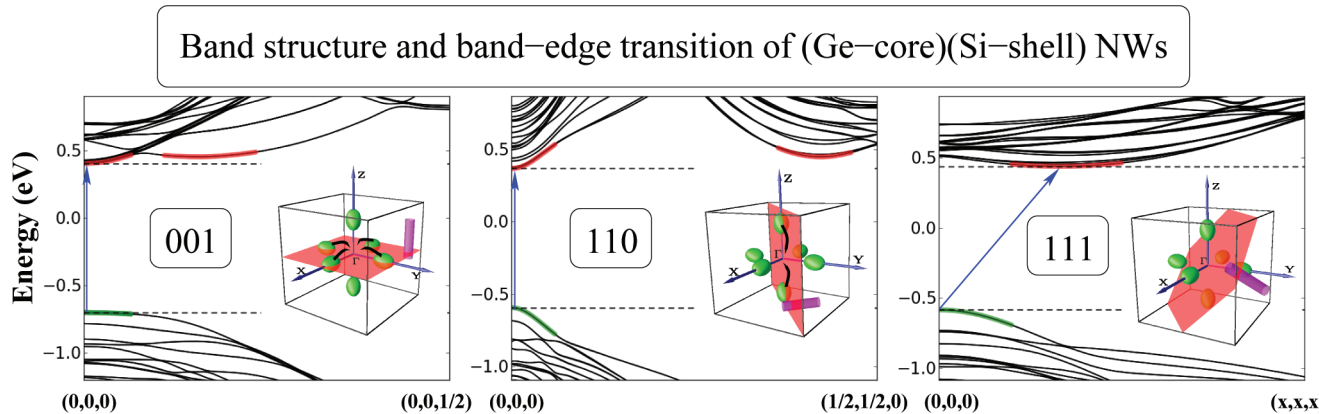


Figure 2. Band structure and band-edge transition of (Ge–core)(Si–shell) NWs along the [001] (left), [110] (middle), and [111] (right) orientation. The (Si–core)(Ge–shell) NWs have similar band structures, where the VBM states originate from Ge region and the CBM states from Si region. The band-edge states are marked in terms of charge localization in Si (red) or Ge (green) region and bandgap transitions are depicted with blue arrows. The zone-boundary value x of [111]-oriented NW is 0.15625. The insets show schematically how Si derived CBM states are formed, i.e., different band-folding behavior of six Δ -valley states of bulk Si along varied NW orientations. For clarity the cubic cell in reciprocal space is shown. The Δ -valley states, NW, and confinement plane are in green, magenta, and red, respectively.

$$\left[-\frac{\hbar^2}{2m} \nabla^2 + \sum_{n,\alpha} v_\alpha(\mathbf{r} - R_{n,\alpha}) + \sum_\alpha V_\alpha^{\text{SO}} \right] \varphi_i(\mathbf{r}) = \varepsilon_i \varphi_i(\mathbf{r}) \quad (1)$$

where the Hamiltonian consists of the kinetic-energy (first term), atomistic screened pseudopotential (second term), and spin-orbit coupling (third term). The screened pseudopotential is fitted to accurately reproduce electronic properties of bulk Si and Ge (e.g., interband transition energies, effective masses, spin-orbit splittings, and deformation potentials), as well as combined Si/Ge systems such as interface band-offsets, and random alloy bowing parameter, thus correcting the well-known “DFT errors” for semiconductors, such as serious underestimation of bandgap and effective mass. This atomistic pseudopotential approach, in conjunction with a folded spectrum method designed to selectively calculate band-edge states,⁴³ enable performing literally millions of calculations with sufficient efficiency for NW systems containing up to 10^5 atoms ($D \approx 8$ nm) during the course of the GA search.

Structure search is performed with a GA approach based on the Darwinian evolution rules of survival of the fittest.^{44–46} Briefly, the initial population of configurations (individuals) is generated randomly. In each evolution step (“generation”) individuals with good target property (“fitness”) survived, a percent of individuals with bad fitness are abandoned, and at the same time new individuals are generated by defined GA operators. For the current topic of searching for bandgap photoluminescence, we defined the fitness of a individual as the oscillator strength of band-edge transitions⁴⁷

$$f_t = \sum_{n_c} \sum_{n_v} f_{cv} = \sum_{n_c} \sum_{n_v} \frac{2|P_{cv}|^2}{m\hbar\omega_{cv}} \quad (2)$$

where $P_{cv} = \langle \varphi_c | \hat{P} | \varphi_v \rangle$, is the dipole matrix element evaluated with the momentum operator for the current periodic system, $\omega_{cv} = E_c - E_v$ represents the transition energy and (n_c, n_v) ((4, 2) is used here) is the number of (conduction, valence) states involved. In addition to GA calculations, we also performed some direct “high-throughput” calculations by directly survey-

ing all of the individuals in designed configuration spaces. The “majority representation” approach⁴⁸ is used to analyze the reciprocal-space projection (onto bulk Bloch states) for the wave functions of band-edge states ($\varphi_i(\mathbf{r})$). Particularly, the projection of $\varphi_i(\mathbf{r})$ at a given translationally invariant wave vector \mathbf{k} in bulk fcc Brillouin zone, $P_i(\mathbf{k})$ is evaluated by

$$P_i(\mathbf{k}) = \sum_{n=1}^{\infty} \langle \varphi_i(\mathbf{r}) | \mathbf{u}_{nk}(\mathbf{r}) e^{ikr} \rangle^2 \quad (3)$$

where $\{\mathbf{u}_{nk}(\mathbf{r}) e^{ikr}\}$ is a complete set of bulk Bloch functions of band index n .

Generic Band Structure of Core/Single-Shell Si/Ge NWs (Figure 2): Direct Bandgap for [001] and [110]-Orientation and Indirect for [111]. To develop basic intuition, we start with the general electronic structure of a core/single-shell NW. The calculated band structures of such NWs oriented along some principle directions are shown in Figure 2. A common feature of different NW orientations is that the VBM wave function is primarily localized on Ge (shown as green) while CBM wave function mainly localized on Si (shown as red).^{49–55} For thick-core/thick-shell NW, this type-II band alignment derives charge separation⁵⁶ and is beneficial to long carrier lifetime but detrimental to strongly radiative electron–hole light-emitting recombination. It can be seen that [001] and [110]-oriented NWs show direct bandgap, whereas [111]-oriented NW is indirect. This can be understood in the framework of band folding that is still approximately valid in large-size nanostructures. In particular, the VBM, which is folded from the Γ_8 of bulk Ge, is always located at $\bar{\Gamma}_h$ of the NW Brillouin-zone, independent of the NW orientation. The CBM is folded from the six Δ_e -valley states of bulk Si, and thus its location in the NW Brillouin-zone depends on the NW orientation (see insets of Figure 2): for [001]-oriented NW, four of the six Δ_e -valley states are involved in the confinement plane, and thus folded to $\bar{\Gamma}_e$. Because their effective mass is higher than that of the two nonfolding states,⁵⁷ as the result of quantum confinement the [001]-oriented NW has direct bandgap. Similarly, for [110]-oriented NW, two of six Δ_e -valley states are folded to $\bar{\Gamma}_e$ forming direct bandgap. In contrast, no Δ_e -valley state is involved in the confinement plane of [111]-oriented NW, and thus all the Δ_e -valley states are

Optimization of oscillator strength: (A-core)(B-shell₁)(A-shell₂) NWs

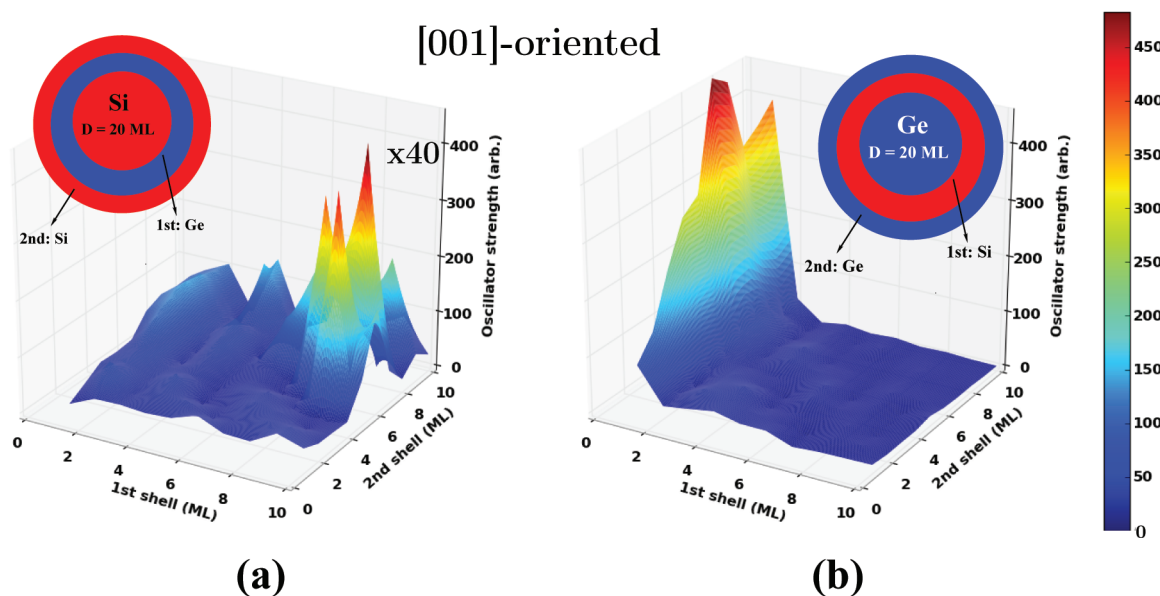


Figure 3. High-throughput calculations of oscillator strength for (Si-core)(Ge-shell₁)(Si-shell₂) (left) and (Ge-core)(Si-shell₁)(Ge-shell₂) (right) NWs oriented along the [001] direction. To adopt the same scale of oscillator strength, the result of (Si-core)(Ge-shell₁)(Si-shell₂) is enlarged by 40 times.

folded to off- $\bar{\Gamma}_e$, leading to indirect bandgap. Although [111]-oriented NWs are the most commonly reported VLS NWs (having the fastest growth rate),^{24–28} we will not consider them further because their bandgap is indirect, which implies weak, phonon-mediated absorption at the band-edges. It should be mentioned that the previous DFT or GW calculations^{49–55} usually consider quite narrow (smaller than 2 nm) NWs due to computational cost. They predicted a formally direct bandgap for [111]-oriented Si NWs⁵⁸ and a formally direct to indirect gap transition depending on composition in [111]-oriented Si/Ge core/shell NWs.⁴⁹ It is important to note that the band-folding often produces formally direct bandgap, but unless the dipole matrix element is explicitly calculated it is not obvious if the corresponding transitions are dipole-allowed (bright) or dipole-forbidden (dark). The results for [111]-oriented ultra narrow NWs are also reproduced by our atomistic pseudopotential calculations, however we find the bandgap transition to be direct but dipole-forbidden, and difficult to be further optimized in the small configuration space (of narrow NWs). In this work, we focus on the thick NWs that are more accessible in current experiments. We aim at seeking the NW geometries that show both direct and bright transitions.

Exploring Basic Trends in [001]-Oriented Si-Core vs Ge-Core NWs with Two Shells Each (Figure 3): Strong Optical Transition in Ge-Core NWs. We performed an exploratory study for the simplest prototype system (Si-core)(Ge-shell₁)(Si-shell₂) and (Ge-core)(Si-shell₁)(Ge-shell₂) NWs oriented along the [001] direction. The core radius is fixed to 10 ML, and we calculate the oscillator strength f_t of eq 2 for varying thickness of the two shells, from 1 to 10 ML, as shown in Figure 3. We observe that

- (i) Ge-core NWs show much larger oscillator strength compared to Si-core NWs.

- (ii) In Ge-core NWs there is a 2 orders of magnitude enhancement of oscillator strength by changing the combination of thicknesses of the two shells, whereas in Si-core NWs the corresponding enhancement is small (within 1 order of magnitude). In Ge-core NWs, the combination of thin Si-shell₁ and thick Ge-shell₂ (i.e., thin Si layers intercalating into thick Ge segments), leads to significant oscillator strength. This interesting result is consistent with the GA search in the rest of the manuscript.

These preliminary high-throughput calculations imply that (i) Ge-core NWs are conducive to strong direct-gap optical transitions, (ii) one can control the optical transition strength by varying the geometry of dual shell structures, (iii) there might be even more opportunity to further improve the transition intensity by using the NW with multiple shells. It was reported by the first-principle calculation⁵⁹ that, with quite weak absorption at the bandgap, pure Ge NWs show the stronger optical activity at 1–2 eV above the bandgap with respect to pure Si NWs. Differently, in the current work we are searching for direct and dipole-allowed transition exactly at the bandgap by exploiting the geometry of core/multishell structure.

GA Search Results (Figure 4) and Best Individuals (Figure 1 and Table 1): Significant Enhancement of Oscillator Strength. We have performed GA searches for core/multishell NWs. Figure 4 illustrates the evolution of fitness (i.e., oscillator strength f_t of eq 2) with generation for [001]-oriented Ge-core NWs. Within less than 50th generation, the best individuals have appeared, and they keep staying superior up to the ~250th generation when new individuals still emerge. This indicates good convergence behavior of GA calculations in the current configuration space.

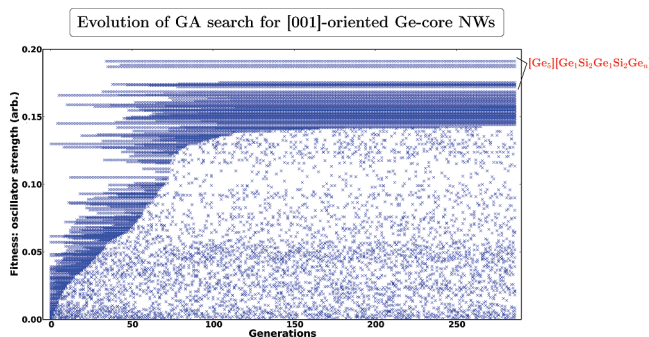


Figure 4. Evolution of fitness (oscillator strength f_t of eq 2) with generation in GA search for [001]-oriented Ge-core NWs. The best individuals (as in the middle of Figure 1) are labeled by separating core and shell regions. The composition formula of best individuals shown represents the sequence of Si/Ge monolayers along the radial direction (starting from the NW axis).

Analysis of GA results indicates that generally the best individual of Si-core NWs exhibits ~ 3 to 4 times smaller oscillator strength than that of Ge-core NWs. Figure 1 and Table 1 describe specific configuration structures and values of oscillator strength for best individuals of [001]-oriented and [110]-oriented Ge-core NWs. For [001]-orientation, the best individual has composition formula $[Ge_5][Ge_1Si_2Ge_1Si_2Ge_n]$ (n is the number of rest shells) (middle of Figure 1). It exhibits 2 orders of magnitude enhancement of oscillator strength (1.9×10^{-1}) by comparison with same-size single-shell (Ge-core)(Si-shell) NW (4.5×10^{-3}), and 3 orders of magnitude enhancement by comparison with same-size pure Si (4.1×10^{-5}) and Ge (2.2×10^{-4}) NW. For [110]-oriented NWs, we found two best individuals with comparable oscillator strength: I, $[Ge_5][Si_1Ge_3Si_2Ge_n]$ (right of Figure 1) and II, $[Ge_5][Ge_4Si_2Ge_n]$. Both show significantly enhanced oscillator strength similar to [001]-oriented NWs. Note that in [110]-orientation the best GA NW II resembles the configuration with the largest oscillator strength in Figure 3(b), i.e., thin Si layers embedded in thick Ge segments as mentioned.

Absorption Sepctra of Best Individuals (Figures 5 and 6): Significantly Enhanced Absorption and Direct-Bandgap Behavior. We calculate the absorption spectrum by involving more near band-edge states with the Fermi's golden rule

$$I(E) = \sum_{n_c} \sum_{n_v} |P_{cv}|^2 \exp\left[-\left(\frac{E - \omega_{cv}}{\sigma}\right)^2\right] \quad (4)$$

where σ (20 meV used here) represents the spectral line broadening, and $n_c = n_v = 50$ in a $1 \times 1 \times 10$ supercell (10 is along the NW orientation). The results of same-size [001] and

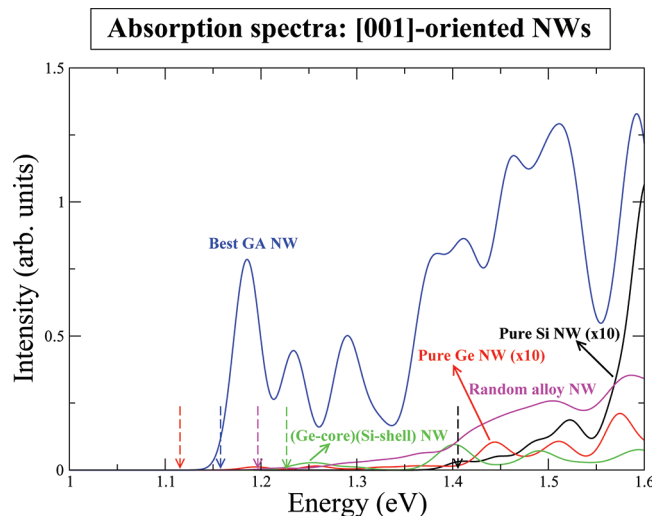


Figure 5. Absorption spectrum of [001]-oriented same-size pure Si NW, pure Ge NW, (Ge-core)(Si-shell) NW (with the same core size as that of best GA NW), random alloy NW (with the same composition as that of best GA NW), and best GA NW (the best individual depicted in Figure 1). The bandgap values are marked with the vertical arrows having consistent color with those of absorption spectra. Some spectra with low intensity (not clearly seen) are amplified.

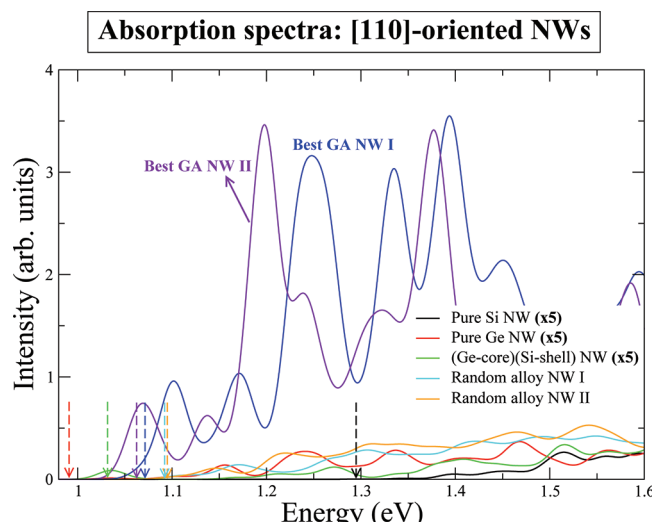


Figure 6. Absorption spectrum of [110]-oriented same-size pure Si NW, pure Ge NW, (Ge-core)(Si-shell) NW (with the same core size as that of best GA NW), random alloy NW I and II (with the same composition as that of best GA NW I and II), and best GA NW I and II (depicted in Figure 1 and Table 1).

Table 1. Calculated Oscillator Strength f_t of eq 2 for Band-Edge Transitions in Same-Size Pure Si NW, Pure Ge NW, (Ge-core)(Si-Shell) NW, and Best GA NWs (the Best Individuals Depicted in Figure 1)^a

[001] NW				
	Si NW	Ge NW	(Ge-core)(Si-shell) NW	best GA NW
oscillator strength (arb.)	4.1×10^{-5}	2.2×10^{-4}	4.5×10^{-3}	1.9×10^{-1}
[110] NW				
	Si NW	Ge NW	(Ge-core)(Si-shell) NW	best GA NW I
oscillator strength (arb.)	2.7×10^{-4}	4.7×10^{-4}	3.4×10^{-3}	2.0×10^{-1}
				1.6×10^{-1}

^aThe (Ge-core)(Si-shell) NW has the same core size as that of best GA NW.

[110]-oriented NWs are shown in Figures 5 and 6, respectively. For both orientations, the absorption spectra of best GA NWs show much stronger optical intensity by more than 1 order of magnitude over other NWs. Especially, for best GA NWs we can clearly see strong absorption peak corresponding to the bandgap transition, indicating direct bandgap behavior. The absorption of random alloy NWs is also much weaker than that of best GA NWs. This indicates that the core/multishell superlattice-like structures are indeed beneficial to the strong optical transition, which can not be simply attributed to the disorder effect. It should be pointed out that these comparisons of absorption spectra are very fair from the viewpoint of theory, since all the NWs have exactly the same size and same numbers of Si + Ge atoms.

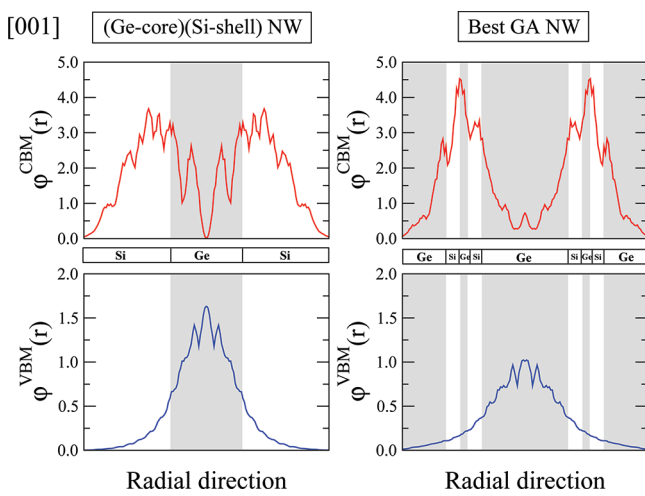


Figure 7. Averaged square of wave function along the radial direction, $|\bar{\varphi}(r)|^2$ for the [001]-oriented same-size (Ge-core)(Si-shell) NW and best GA NW. $|\bar{\varphi}(r)|^2$ is calculated by integrating square of wave function, $|\varphi(r,\theta,l)|^2$ along the tangential direction, θ and NW axis, l , i.e., $|\bar{\varphi}(r)|^2 = \int |\varphi(r,\theta,l)|^2 d\theta dl$. White and gray background corresponds to Si and Ge region, respectively.

Analysis of Charge Distribution (Figure 7) and Orbital Character (Figure 8) of Band-Edge States: What Is Responsible for the Significant Enhancement of Direct-Gap Transitions? To probe the underlying mechanism of the

remarkably enhanced dipole-allowed transition in the best GA NWs, we performed further analysis on the wave functions of band-edge states. Figure 7 shows the real-space radial distribution of wave function square (charge) in [001]-oriented best GA NW ($[Ge_s][Ge_1Si_2Ge_1Si_2Ge_n]$), comparing with that of (Ge-core)(Si-shell) NW. As seen, in the best GA NW the CBM state concentrates more around the region of thin Si layers, and the VBM is mainly located in Ge cores. There is no obvious increase in overlap between the CBM and VBM states in best GA NW. So the real-space analysis does not disclose the reason for optical enhancement.

We then analyze in Figure 8 the reciprocal-space projection, i.e. the percent of bulk Bloch states mixed into the NW CBM, for [001]-oriented pure Si, (Ge-core)(Si-shell) and best GA NW. Reciprocal-space analysis is asking how much Γ , X , L ... character from the bulk Si and Ge are mixed into the NW CBM and VBM. Since the NW VBM is Γ -like as mentioned, we are interested in maximizing bulk Γ character into the NW CBM. Consistent with the above band-folding analysis, in all the NWs the CBM originates mainly from four of six Δ_e -valley states. However, moving on from the left (pure Si NW), middle ((Ge-core)(Si-shell) NW), to right (best GA NW) panel, one clearly observes improved content between Δ_e and Γ_e , and content of Γ_e . This indicates the strongly increased hybridization between the Δ_e and Γ_e states in best GA NW. The CBM state with this hybridization can interact with VBM from Γ_h , leading to strong dipole transition matrix element. Therefore, it is the increased $\Delta_e - \Gamma_e$ interband coupling in the CBM state that is responsible for the strong dipole-allowed transition in best GA NW. The GA calculation is actually to maximize this $\Delta_e - \Gamma_e$ hybridization/coupling by varying the composition of Si and Ge subshells.

The above analysis implies that, to gain strong direct-gap transition in the Si/Ge system, we need to provide some engineering (through the effect of strain, quantum confinement, interstate mixing, etc.) for the predominately Si-derived CBM state. This explains why Ge-core NWs are better than Si-core NWs: in Si-core NWs, the CBM is primarily originated from the thick Si-core region. The engineering for the CBM, which can be afforded by varying multiple shells, is limited, and thus the corresponding enhancement of optical transition is small. The above mechanism (i.e., the hybridization with Γ -like state in the CBM) responsible for strong direct-gap transition

Majority representation of [001]-oriented NWs

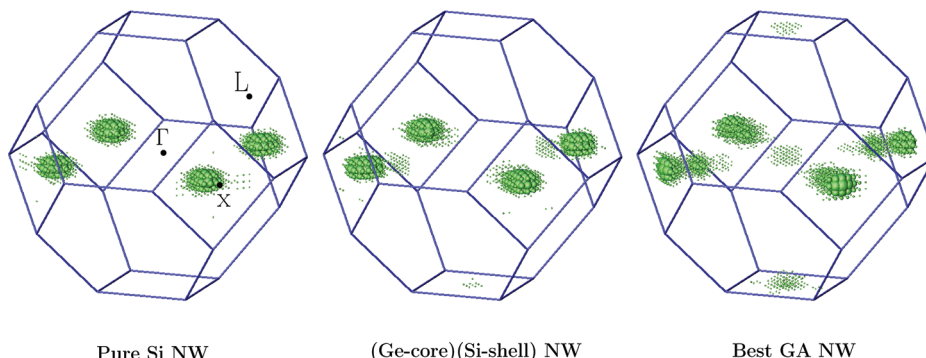


Figure 8. Reciprocal-space projection of the CBM state for same-size pure Si NW, (Ge-core)(Si-shell) NW, and best GA NW oriented along [001] direction, as obtained from the majority representation⁴⁸ in fcc Brillouin zone.

in Ge-core NWs may also adapt to the origin of the stronger optical activity at 1–2 eV above the bandgap in pure Ge NWs.⁵⁹

Compromising with Geometric Parameters Currently Realizable by Experimental Condition: Effect of Increasing Thickness of Thin Si/Ge Shells (Figures 9 and 10): How Much Transition Intensity Do We Lose? In both [001]-oriented and [110]-oriented NWs, the best individuals discovered from the GA search (Figure 1) have in common narrow (1–2 ML) Si shells. The well-controlled growth of such thin monatomic-layer in core/multishell NWs is still a challenge for current VLS-based technique, although a 2–3 Å layer-by-layer growth has been recently accomplished by Ben-Ishai et al.²⁸ Considering this current experimental limitation to not very thin shells, we design a calculation to study the effect of increasing thickness of the thin Si layer in the NW structure

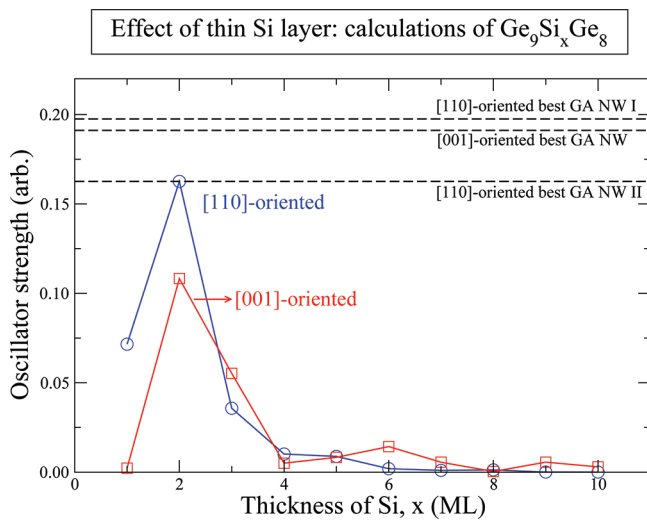


Figure 9. Evolution of oscillator strength with increasing thickness of Si shell in [001] and [110]-oriented NWs with thin Si shell embedded in thicker Ge region, $\text{Ge}_9\text{Si}_x\text{Ge}_8$ ($x = 1\text{--}10$ ML). The oscillator strength of best GA NWs is shown.

with a narrow Si shell embedded in wide Ge regions, as in Figure 9. We find that actually the highest oscillator strength always occurs at 2 ML rather than the smallest 1 ML. When the thickness of thin Si layer increases from 2 to 4 ML (equal to a_{bulk}), the oscillator strength is reduced by about 1 order of magnitude. However, the corresponding value is still much larger than that of pure Si NW, pure Ge NW, and (Ge-core)(Si-shell) NW (Table 1).

We have performed additional high-throughput calculations for [001]-oriented NWs with the larger thickness (2 and 4 ML) of individual Si/Ge shell. The results are compared with those of random alloy NWs in Figure 10. It can be seen again that Ge-core NWs (right) give (more than 5 times) larger oscillator strength than Si-core NWs (left). For the 4-ML-shell NWs, the oscillator strength is generally lower than that of random alloy NWs. Turning to the 2-ML-shell NWs, Ge-core NWs show rather larger oscillator strength than that of random alloy NWs, and in Si-core NWs they are comparable. The common feature of the 2-ML-shell Ge-core NWs having high oscillator strength is the appearance of thin Si layer, which again indicates the important role of thin Si layer in producing strong optical transition.

■ SUMMARY

In summary, we present a genomic search for both a direct gap and a strong dipole-allowed optical transition in the one-dimensional Si/Ge heterostructures, coaxial core-multishell nanowires (NWs), by using a combination of a genetic algorithm with the atomistic pseudopotential electronic-structure calculations. The configuration space used spans all geometric parameters of this system, including the NW orientation, material of core and shells, shell sequence, and shell thickness, etc. We find from our results the following design principles: (i) Ge-core NWs have better performance than Si-core NWs on enhancing direct-gap optical transition, (ii) [001] and [110]-oriented NWs can have direct bandgap, whereas [111]-oriented NWs do not, (iii) the core/multishell NWs can offer greater optical transitions by more than an order of magnitude over pure Si, Ge, core/single-shell, and homogeneous alloy NWs, (iv) the winning configurations

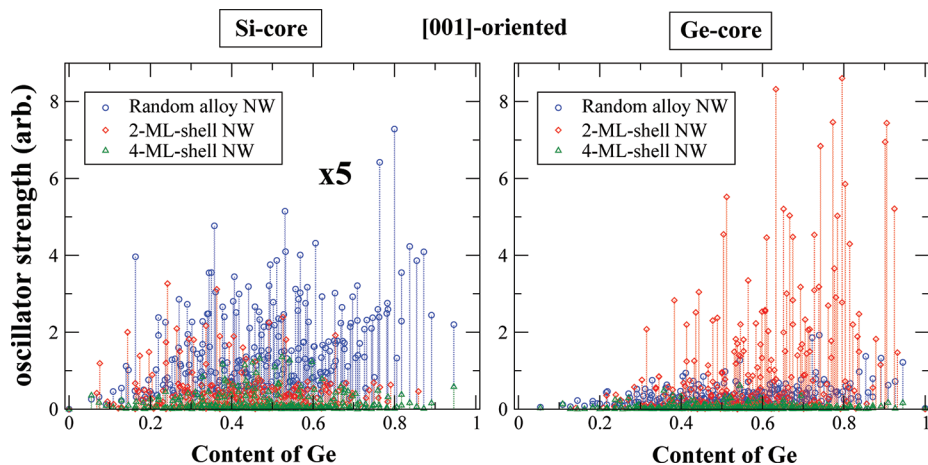


Figure 10. Direct high-throughput calculations for [001]-oriented core-multishell NWs with larger thickness of each shell. The core size, R_{core} is fixed to 10 ML and eight shells are surrounded. The thickness of each shell is in unit of 2 ML (2-ML-shell NW) and 4 ML (4-ML-shell NW). Each shell can be either Si or Ge, and thus we have 2^8 individuals for both Si-core (left) and Ge-core (right) case. The results of random alloy NWs (with the same composition as those of 4-ML-shell NWs) are shown for comparison. Note that here the random alloy NWs are still periodic along the NW axis, and thus are not strictly “random alloy”. The results of Si-core are amplified (by 5 times) to be clearly seen.

with the strongest oscillator strength are $[Ge_5][Ge_1Si_2Ge_1Si_2Ge_n]$ for [001]-oriented NWs, as well as $[Ge_5][Si_1Ge_3Si_2Ge_n]$ and $[Ge_5][Ge_4Si_2Ge_n]$ for [110]-oriented NWs, (v) significantly enhanced optical transitions are found for rather narrow Si layer embedded in wide Ge shells, (vi) the mixing of bulk Γ -like state into the Δ -dominated conduction band minimum of NWs is responsible for the strong direct-gap transition. The present study offers an attractive perspective to gain strongly efficient light-emitting properties based on Si/Ge materials by further engineering this one-dimensional core/multishell nanowire system.

AUTHOR INFORMATION

Corresponding Author

*E-mail: lijun_physics@yahoo.com.cn; alex.zunger@gmail.com.

ACKNOWLEDGMENTS

A.Z. thanks Fernando Patolsky and Ori Cheshnovsky of Tel Aviv University for important discussions on core/multishell Si-Ge nanowires. This work is supported by the U.S. Department of Energy, Office of Science, Basic Energy Sciences, under Contract No. DE-AC36-08GO28308 to NREL. The “Center for Inverse Design” is a DOE Energy Frontier Research Center. The use of MPP capabilities at the National Energy Research Scientific Computing Center is gratefully acknowledged.

REFERENCES

- (1) Ossicini, S.; Pavesi, L.; Priolo, F. Light emitting silicon for microphotonics. Springer Tracts on Modern Physics No. 194; Springer-Verlag: Berlin, 2003.
- (2) Pavesi, L.; Lockwood, D. J. Silicon photonics. Topics in Applied Physics No. 94; Springer-Verlag: Berlin, 2004.
- (3) Pearsall, T. P.; Bevk, J.; Feldman, L. C.; Bonar, J. M.; Mannaerts, J. P.; Ourmazd, A. *Phys. Rev. Lett.* **1987**, *58*, 729–732.
- (4) Zachai, R.; Eberl, K.; Abstreiter, G.; Kasper, E.; Kibbel, H. *Phys. Rev. Lett.* **1990**, *64*, 1055–1058.
- (5) Menczigar, U.; Abstreiter, G.; Olajos, J.; Grimmmeiss, H.; Kibbel, H.; Presting, H.; Kasper, E. *Phys. Rev. B* **1993**, *47*, 4099–4102.
- (6) Soref, R. A. *Proc. IEEE* **1993**, *81*, 1687–1706.
- (7) Green, M. A.; Zhao, J.; Wang, A.; Reece, P. J.; Gal, M. *Nature* **2001**, *412*, 805–808.
- (8) Gudiksen, M.; Lauhon, L.; Wang, J.; Smith, D.; Lieber, C. *Nature* **2002**, *415*, 617–620.
- (9) Bonfanti, M.; Grilli, E.; Guzzi, M.; Virgilio, M.; Grossi, G.; Chrastina, D.; Isella, G.; von Känel, H.; Neels, A. *Phys. Rev. B* **2008**, *78*, 041407.
- (10) Sun, X.; Liu, J.; Kimerling, L. C.; Michel, J. *Opt. Lett.* **2009**, *34*, 1198–+.
- (11) Kelzenberg, M.; Boettcher, S.; Petykiewicz, J.; Turner-Evans, D.; Putnam, M.; Warren, E.; Spurgeon, J.; Briggs, R.; Lewis, N.; Atwater, H. *Nat. Mater.* **2010**, *9*, 239–244.
- (12) Nataraj, L.; Xu, F.; Cloutier, S. G. *Opt. Express* **2010**, *18*, 7085–7091.
- (13) Gnutzmann, U.; Clausecker, K. *Appl. Phys.* **1974**, *3*, 9–14.
- (14) Hybertsen, M. S.; Schlüter, M. *Phys. Rev. B* **1987**, *36*, 9683–9693.
- (15) Schmid, U.; Christensen, N. E.; Alouani, M.; Cardona, M. *Phys. Rev. B* **1991**, *43*, 14597–14614.
- (16) Carroll, L.; Imbert, F.; Sigg, H.; Süess, M.; Müller, E.; Virgilio, M.; Pizzi, G.; Rossbach, P.; Chrastina, D.; Isella, G. *Appl. Phys. Lett.* **2011**, *99*, 031907.
- (17) d’Avezac, M.; Luo, J. W.; Chanier, T.; Zunger, A. *Phys. Rev. Lett.* in press.
- (18) People, R.; Bean, J. C. *Appl. Phys. Lett.* **1985**, *47*, 322–324.
- (19) Ertekin, E.; Greaney, P. A.; Chrzan, D. C.; Sands, T. D. *J. Appl. Phys.* **2005**, *97*, 114325–+.
- (20) Kavanagh, K. L. *Semicond. Sci. Technol.* **2010**, *25*, 024006.
- (21) Wagner, R. S.; Ellis, W. C. *Appl. Phys. Lett.* **1964**, *4*, 89–90.
- (22) Morales, A. M.; Lieber, C. M. *Science* **1998**, *279*, 208–+.
- (23) Duan, X.; Lieber, C. M. *Adv. Mater.* **2000**, *12*, 298–302.
- (24) Lauhon, L. J.; Gudiksen, M. S.; Wang, D.; Lieber, C. M. *Nature* **2002**, *420*, 57–61.
- (25) Goldthorpe, I. A.; Marshall, A. F.; McIntyre, P. C. *Nano Lett.* **2009**, *9*, 3715–3719, PMID: 19795838
- (26) Xiang, J.; Lu, W.; Hu, Y.; Wu, Y.; Yan, H.; Lieber, C. M. *Nature* **2006**, *441*, 489–493.
- (27) Dayeh, S. A.; Gin, A. V.; Picraux, S. T. *Appl. Phys. Lett.* **2011**, *98*, 163112.
- (28) Ben-Ishai, M.; Patolsky, F. *Adv. Mater.* **2010**, *22*, 902–+.
- (29) Maeda, Y.; Tsukamoto, N.; Yazawa, Y.; Kanemitsu, Y.; Masumoto, Y. *Appl. Phys. Lett.* **1991**, *59*, 3168–3170.
- (30) Takagahara, T.; Takeda, K. *Phys. Rev. B* **1992**, *46*, 15578–15581.
- (31) Delerue, C.; Allan, G.; Lannoo, M. *Phys. Rev. B* **1993**, *48*, 11024–11036.
- (32) Qi, J.; Belcher, A. M.; White, J. M. *Appl. Phys. Lett.* **2003**, *82*, 2616–2618.
- (33) Ma, D. D. D.; Lee, S. T.; Shinar, J. *Appl. Phys. Lett.* **2005**, *87*, 033107–+.
- (34) Dovrat, M.; Arad, N.; Zhang, X.-H.; Lee, S.-T.; Sa’ar, A. *Phys. Rev. B* **2007**, *75*, 205343.
- (35) Guichard, A. R.; Barsic, D. N.; Sharma, S.; Kamins, T. I.; Brongersma, M. L. *Nano Lett.* **2006**, *6*, 2140–2144.
- (36) Walavalkar, S. S.; Hofmann, C. E.; Homyk, A. P.; Henry, M. D.; Atwater, H. A.; Scherer, A. *Nano Lett.* **2010**, *10*, 4423–4428.
- (37) Valenta, J.; Bruhn, B.; Linnros, J. *Nano Lett.* **2011**, *11*, 3003–3009.
- (38) Audit, G.; Mhuircheartaigh, É.; Lipson, S.; Morris, M.; Blau, W.; Holmes, J. J. *Mater. Chem.* **2005**, *15*, 4809–4815.
- (39) Guichard, A. R.; Kekatpure, R. D.; Brongersma, M. L.; Kamins, T. I. *Phys. Rev. B* **2008**, *78*, 235422.
- (40) Wang, J.; Gudiksen, M. S.; Duan, X.; Cui, Y.; Lieber, C. M. *Science* **2001**, *293*, 1455–1457.
- (41) Bernard, J. E.; Zunger, A. *Phys. Rev. B* **1991**, *44*, 1663–1681.
- (42) Zunger, A. *First Principles and Second Principles Pseudopotentials*; Chelikowsky, J. R., Louie, S. G., Eds.; Kluger Academic: Boston, MA, 1996; pp 173–187.
- (43) Wang, L.; Zunger, A. *J. Chem. Phys.* **1994**, *100*, 2394.
- (44) Kim, K.; Graf, P. A.; Jones, W. B. *J. Comput. Phys.* **2005**, *208*, 735–760.
- (45) Franceschetti, A.; Zunger, A. *Nature* **1999**, *402*, 60–63.
- (46) Piquini, P.; Graf, P. A.; Zunger, A. *Phys. Rev. Lett.* **2008**, *100*, 186403–+.
- (47) Yu, P. Y.; Cardona, M. *Fundamentals of Semiconductors: Physics and Materials Properties*; Springer-Verlag: Berlin, Heidelberg, 2010.
- (48) Wang, L.-W.; Bellaiche, L.; Wei, S.-H.; Zunger, A. *Phys. Rev. Lett.* **1998**, *80*, 4725–4728.
- (49) Musin, R. N.; Wang, X.-Q. *Phys. Rev. B* **2005**, *71*, 155318.
- (50) Peköz, R.; Raty, J.-Y. *Phys. Rev. B* **2009**, *80*, 155432.
- (51) Peelaers, H.; Partoens, B.; Peeters, F. M. *Phys. Rev. B* **2010**, *82*, 113411.
- (52) Peng, X.; Logan, P. *Appl. Phys. Lett.* **2010**, *96*, 143119.
- (53) Amato, M.; Palummo, M.; Ossicini, S. *Phys. Rev. B* **2009**, *79*, 201302.
- (54) Amato, M.; Palummo, M.; Ossicini, S. *Phys. Rev. B* **2009**, *80*, 235333.
- (55) Amato, M.; Ossicini, S.; Rurali, R. *Nano Lett.* **2011**, *11*, 594–598.
- (56) Nduwimana, A.; Musin, R. N.; Smith, A. M.; Wang, X.-Q. *Nano Lett.* **2008**, *8*, 3341–3344.
- (57) Rurali, R. *Rev. Mod. Phys.* **2010**, *82*, 427–449.
- (58) Zhao, X.; Wei, C. M.; Yang, L.; Chou, M. Y. *Phys. Rev. Lett.* **2004**, *92*, 236805.
- (59) Bruno, M.; Palummo, M.; Marini, A.; Del Sole, R.; Olevano, V.; Kholid, A. N.; Ossicini, S. *Phys. Rev. B* **2005**, *72*, 153310.